Monthly Notices
of the
ROYAL ASTRONOMICAL SOCIETY

MNRAS **492,** 2405–2417 (2020)
Advance Access publication 2020 January 8

doi:10.1093/mnras/staa015

# A spectroscopic survey of Abell 1703: is it a rare relaxed cluster hosting a radio halo or a usual merging system?

W. Boschin,[1,2,3]★ M. Girardi[4,5] and F. Gastaldello[6]

[1]*Fundación G. Galilei - INAF (Telescopio Nazionale Galileo), Rambla J. A. Fernández Pérez 7, E-38712 Breña Baja (La Palma), Spain*
[2]*Instituto de Astrofísica de Canarias, C/Vía Láctea s/n, E-38205 La Laguna (Tenerife), Spain*
[3]*Departamento de Astrofísica, Univ. de La Laguna, Av. del Astrofísico Francisco Sánchez s/n, E-38205 La Laguna (Tenerife), Spain*
[4]*Dipartimento di Fisica dell'Università degli Studi di Trieste - Sezione di Astronomia, via Tiepolo 11, I-34143 Trieste, Italy*
[5]*INAF - Osservatorio Astronomico di Trieste, via Tiepolo 11, I-34143 Trieste, Italy*
[6]*INAF - IASF Milano, via E. Bassini 15, I-20133 Milano, Italy*

Accepted 2019 December 24. Received 2019 November 27; in original form 2019 October 15

## ABSTRACT

We present the study of the internal dynamics of the intriguing galaxy cluster Abell 1703, a system hosting a probable giant radio halo whose dynamical status is still controversial. Our analysis is based on unpublished spectroscopic data acquired at the Italian Telescopio Nazionale *Galileo* and data publicly available in the literature. We also use photometric data from the Sloan Digital Sky Survey. We select 147 cluster members and compute the cluster redshift $\langle z \rangle \sim 0.277$ and the global line-of-sight velocity dispersion $\sigma_v \sim 1300\,\mathrm{km\,s^{-1}}$. We infer that Abell 1703 is a massive cluster: $M_{200} \sim 1$–$2 \times 10^{15}\,\mathrm{M_\odot}$. The results of our study disagree with the picture of an unimodal, relaxed cluster as suggested by previous studies based on the gravitational lensing analysis and support the view of a perturbed dynamics proposed by recent works based on *Chandra* X-ray data. The first strong evidence of a dynamically disturbed cluster comes from the peculiarity of the BCG velocity with respect to the first moment of the velocity distribution of member galaxies. Moreover, several statistical tests employed to study the cluster galaxies kinematics find significant evidence of substructure, being Abell 1703 composed by at least two or three subclumps probably caught after the core–core passage. In this observational scenario, the suspected existence of a radio halo in the centre of this cluster is not surprising and well agrees with the theoretical models describing diffuse radio sources in clusters.

**Key words:** galaxies: clusters: general – galaxies: clusters: individual: Abell 1703 – galaxies: kinematics and dynamics.

## 1 INTRODUCTION

*Radio haloes* (also *giant radio haloes*, or GRHs) are diffuse sources found in the central regions of massive ($M_{200} \gtrsim 10^{15}\,\mathrm{M_\odot}$) galaxy clusters. Extended over volumes of $\sim$1 Mpc$^3$, these low surface brightness features ($\sim$1 μJy arcsec$^{-2}$ at 1.4 GHz) have no obvious optical counterparts and roughly follow the intracluster medium (ICM) mass distribution. Their synchrotron steep-spectrum ($S(\nu) \sim \nu^{-\alpha}$; $\alpha > 1$) reveals the existence of a population of relativistic electrons and large-scale magnetic fields spread throughout the ICM (see e.g. Feretti et al. 2012 for a review).

Until recently, GRHs were always discovered in merging clusters (e.g. van Weeren et al. 2019). Indeed, in the hierarchical scenario of cosmic structure formation, it is a common fact that galaxy groups and subclusters merge together into massive clusters. These processes release enormous amounts of gravitational energy (as large as $10^{64}$ erg; Sarazin 2002) and induce turbulence in the ICM, which is considered the key mechanism able to accelerate particles to relativistic energies (e.g. Brunetti & Jones 2015).

However, in the last years this picture got more complicated following the discovery of diffuse radio emission in several dynamically relaxed clusters. The first, impacting, case was the extended radio source found in the cluster CL1821 + 643 ($z \sim 0.296$; Bonafede et al. 2014, Boschin et al. 2018), whose size, location, and power resemble that of typical GRHs despite the absence of any merging process responsible for its formation. Indeed, this case is not unique, since diffuse radio sources not powered by major mergers have been recently discovered in more clusters in the redshift range 0.1–0.3. For instance, Abell 2390 and Abell 2261 (Sommer et al. 2017) are two more examples of cool-core clusters with Mpc-scale radio sources. Intriguing are also the cases

★ E-mail: boschin@tng.iac.es

of PSZ1G139.61 + 24 and Abell 2142. The first one hosts both a mini-halo (a feature typically found in cool-core relaxed systems, e.g. Gitti et al. 2018) and an underluminous and ultrasteep spectrum radio halo (Savini et al. 2018a). Abell 2142, on its hand, is affected by minor merging activity, as suggested by the cold fronts detected in its ICM. However, as in the case of PSZ1G139.61 + 24, it also exhibits a double-component extended radio emission (Venturi et al. 2017), with a spectral steepness increasing in the outer regions. These two last examples could be hybrid sources, with mini-haloes evolving into GRHs or vice versa (van Weeren et al. 2019). It is expected that the number of these 'intermediate' cases will increase considerably in the near future thanks to observational facilities like LOFAR (van Haarlem et al. 2013).

Taking into account this new framework, in this paper we focus on Abell 1703 (hereafter A1703; Abell 1958, Abell, Corwin & Olowin 1989), a system at $z \sim 0.28$ (Allen et al. 1992) whose dynamical status and radio properties might look like the ones of CL1821 + 643. In fact, several authors claim the possible existence of a radio halo in this cluster. The first hint comes from Owen, Morrison & Voges (1999; see their table 2), who include A1703 in a list of nine clusters with diffuse radio emission. Indeed, A1703 is the brightest source in Owen et al. sample. More recently, the analysis of archival VLA data at 1.4 GHz showed some evidence of diffuse emission in the central region of the cluster (Govoni, private communication; see also our Fig. 1) despite contamination by radio point-like sources (see Rizza et al. 2003 and our Section 2.1). Finally, Wilber (2018) highlights the presence in A1703 of possible radio halo emission at lower frequencies (120–168 MHz) in the LOFAR Two-Metre Sky Survey (LoTSS). This evidence is also confirmed by Savini et al. (2018b) in their fig. 8, where the contour levels at 144 MHz from LOFAR suggest the existence of a diffuse source in the location of the cluster.

On the other hand, the picture of A1703 that emerges at other wavelengths is controversial and suggest conflicting interpretations about the real dynamical status of this cluster. From the optical point of view A1703 is one of the richest clusters in the photometric catalogue of the SDSS (e.g. Koester et al. 2007) and presents a dominant giant elliptical cD galaxy in its centre (the brightest cluster galaxy; hereafter BCG). Moreover, this cluster shows impressive strong gravitational lensing features (Hennawi et al. 2008) which allowed to reconstruct its internal mass profile. For instance, Limousin et al. (2008), based on imaging data both from space (*HST*) and ground (Subaru), identified 13 systems forming highly magnified images. Thanks to spectroscopic (from Keck) and photometric redshifts of these images they found that all the lensing systems can be reproduced by a single NFW (Navarro, Frenk & White 1997) profile for the dark matter, thus suggesting that A1703 is a regular, unimodal cluster. A follow-up study by Richard et al. (2009) based on further Keck spectroscopic measurements for seven multiple sources reinforced the evidence that A1703 is a relaxed cluster. More studies based on strong and/or weak gravitational lensing analysis also provided estimates of the cluster mass and the NFW concentration parameter. Even though the results are quite discordant, they all coincide that A1703 is a massive system: $M_{\rm vir} \simeq 1.1$–$2 \times 10^{15}\,{\rm M}_{\odot}$ and $c_{\rm vir} \simeq 3.3$–$7.1$ (Oguri et al. 2009, Zitrin et al. 2010, Oguri et al. 2012).

Such a large mass is also consistent with estimates derived from *Planck* observations of the thermal Sunyaev–Zeldovich effect. In fact, based on measurements of the Compton parameter $Y$ and the $Y - M_{500}$ scaling relation of Arnaud et al. (2010), the Planck Collaboration XIII (2016) reports an hydrostatic mass $M_{500}^{\rm SZ} = 6.76^{+0.35}_{-0.37} \times 10^{14}\,{\rm M}_{\odot}$, which corresponds to $M_{\rm vir} \gtrsim 1 \times 10^{15}\,{\rm M}_{\odot}$ assuming an NFW profile for the mass distribution.

As for the X-ray band, Piffaretti et al. (2011) report a measurement of the X-ray luminosity of A1703 from *ROSAT* data: $L_{\rm X}(R < R_{500} = 1.07\ {\rm Mpc}) = 5.42 \times 10^{44}\,{\rm erg\,s^{-1}}$ in the 0.1–2.4 keV band. Using equation (10) of Böhringer, Chon & Collins (2014), this luminosity translates to a mass estimate $M_{200} \gtrsim 1 \times 10^{15}\,{\rm M}_{\odot}$ (in our cosmology, see below), again indicative of a massive cluster. Very recently, Ge et al. (2019) used unpublished *Chandra* archival data to compute the temperature of the ICM within 0.15–0.75 $R_{500}$: $kT_{\rm X} = 9.63 \pm 0.75$ keV. These data show that the ICM is elongated in the SSE-NNW direction (see contours in Fig. 1). However, despite the absence of obvious bimodality or more complex substructure, Ge et al. (2019) also report hints of a disturbed dynamics according to the measurements of several X-ray morphological parameters (see their table 5) and their locations in the morphological planes of Cassano et al. (2010) and Mantz et al. (2015).

Taking into account the scenarios described by studies based on gravitational lensing and X-ray data, it is important to definitively establish whether A1703 is an anomalous relaxed cluster hosting diffuse radio emission or a common merging system. An exhaustive analysis of the kinematics of the cluster galaxy population could have the last word on the true dynamical status of this cluster. Moreover, this analysis would allow to study the possible presence of a merger along the line of sight, which would be difficult if not impossible to detect in the X-ray band. In fact, the spatial and kinematical study of member galaxies represent an effective tool to reveal substructures in clusters and put in evidence pre-merging subgroups or merger remnants (e.g. Boschin et al. 2004; Boschin, Girardi & Barrena 2013).

With this context in mind, we used archival spectroscopic data obtained at the Italian Telescopio Nazionale *Galileo* (TNG) in order to perform the first dynamical analysis of this cluster based on member galaxies. These data sample the central ∼1 Mpc size region of the cluster characterized by the diffuse X-ray and radio emissions. More data found in the NED Data base, most of which obtained by Bayliss et al. (2014; hereafter B14) through spectroscopic measurements with MMT/Hectospec, allowed us to extend our spectroscopic sample to cover a wider area around the cluster (see Fig. 2).

This paper is organized as follows. Section 2 describes the TNG observations and data reduction and presents the velocity catalogue. In Section 3 we describe our member selection procedure. Sections 4 and 5 explain the results of the analysis of the cluster structure. Finally, in Section 6, we discuss our results and present a portrait of the dynamical status of A1703.

Unless otherwise stated, we indicate errors at the 68 per cent confidence level (hereafter c.l.). Throughout this paper, we use $H_0 = 70\ {\rm km\,s^{-1}\,Mpc^{-1}}$ in a flat cosmology with $\Omega_{\rm m} = 0.3$ and $\Omega_{\Lambda} = 0.7$. In the adopted cosmology, 1 arcmin corresponds to ∼253 kpc at the cluster redshift.

## 2 GALAXY DATA AND VELOCITY CATALOGUE

We used unpublished spectroscopic data stored in the TNG archive (http://archives.ia2.inaf.it/tng) taken in 2010 May (program A21TAC_50; PI: F. Gastaldello). These data consist of five MOS masks mainly sampling the central region of the cluster. Another mask was taken in 2016 June during a technical night. In particular,

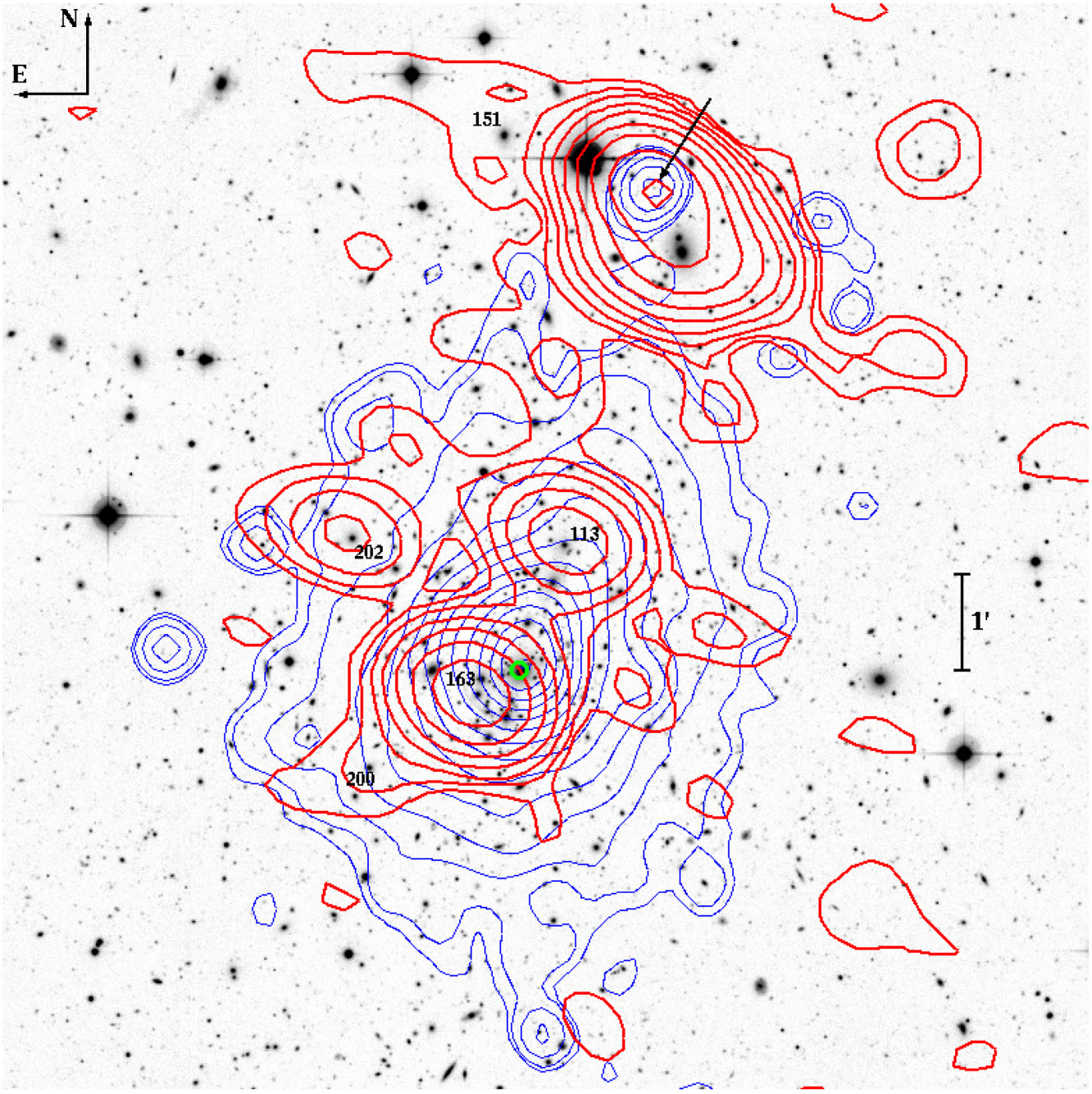


**Figure 1.** A multiwavelength picture of the cluster A1703. The grey-scale image in the background corresponds to the optical *r*-band (CFHT/Megaprime archival data). The blue thin contours show the cluster X-ray emission in the 0.5–2 keV band (from *Chandra* archival image ID 16126; Texp: 48 ks). The thick red contours are the contour levels of a VLA 1.4 GHz low-resolution image (courtesy F. Govoni; from archival VLA observation program AM 469). Numbers highlight member galaxies mentioned in the text. The green circle is the BCG (ID 141; see Table 1).

this last mask allowed us to obtain the spectrum of the BCG. For all the six masks we used the LR-B Grism of the instrument DOLoRes[1] and obtained spectra for 131 objects. The total exposure times varied from 3600 to 7200 s.

We used standard IRAF tasks to reduce the spectra and adopted the cross-correlation technique (Tonry & Davis 1979) to compute redshifts for 104 targets. For 18 galaxies we obtained multiple redshift determinations. They allowed us to obtain a better estimate for the redshift errors. In particular, we found that the nominal cross-correlation errors are underestimated and multiplied them by a factor 2.5 (see Girardi et al. 2011 for details of the redshift computation and their errors). For another five galaxies (IDs. 117, 152, 154, 162, and 180; see Table 1), their redshifts were computed by measuring the wavelengths of the emission lines in their spectra.

In order to extend our spectroscopic sample to the outskirts of the cluster, we searched the NED data base for galaxies with known

[1]http://www.tng.iac.es/instruments/lrs

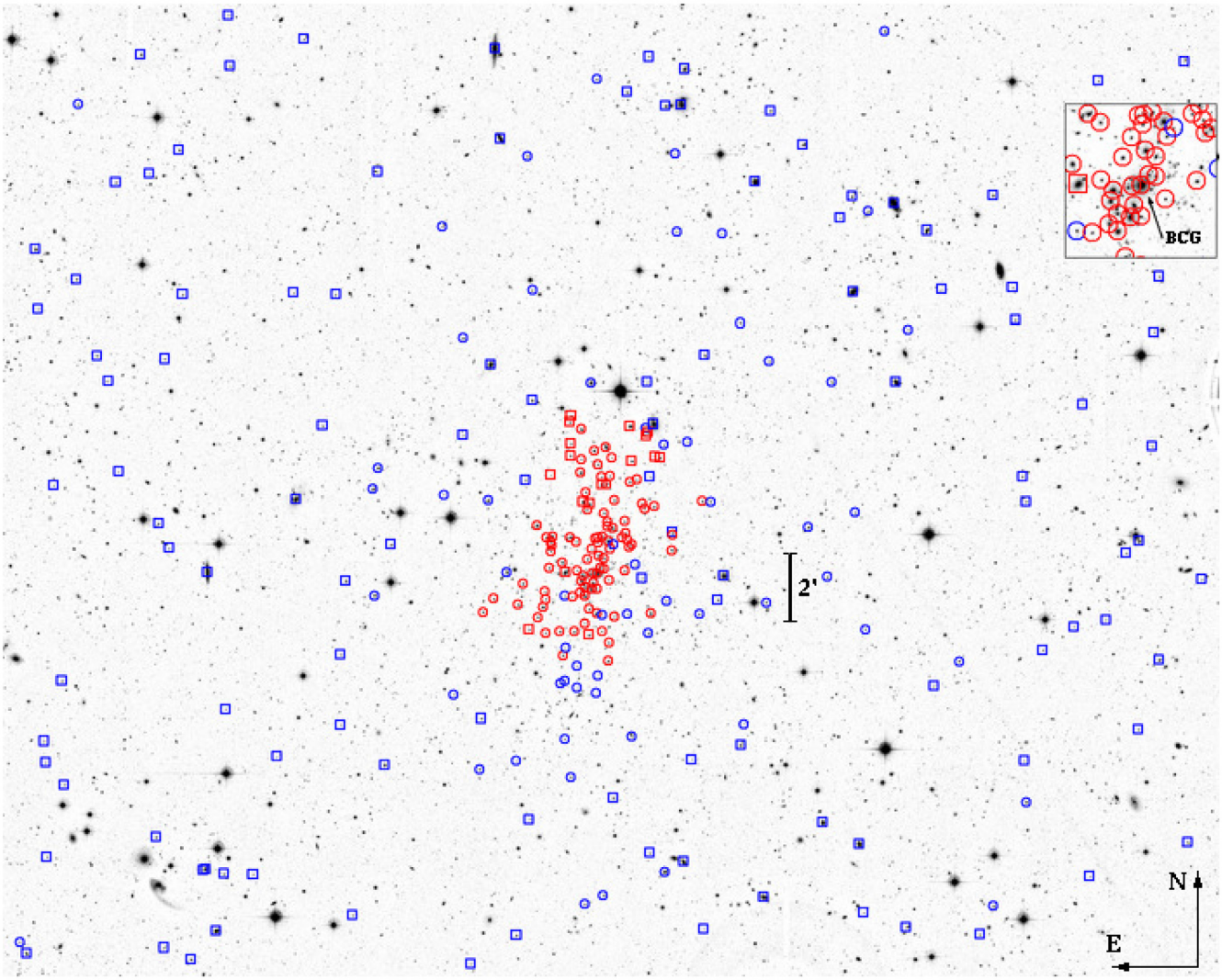


**Figure 2.** *r*-band wide field image (CFHT/Megaprime archival data) of the cluster A1703 showing the positions of all the galaxies of our spectroscopic catalogue. The circles and squares indicate cluster members and non-member galaxies, respectively. The red symbols refer to galaxies observed at the TNG (see the text and Table 1). Top right inset is a zoom on the central region of the cluster.

redshift in the field of A1703. We found 184 objects within a radius of ∼20 arcmin from the cluster centre. Most of these objects (177) come from B14, ten of which are in common with our TNG data. To check for eventual systematic deviations, we performed a straight-line fit to the TNG and B14 redshift measurements taking into account the errors on both data sets (see chapter 15.3 of Press et al. 2007). We find an intercept $= (-2 \pm 8) \times 10^{-3}$ and a slope $= 1.01 \pm 0.03$ with a $\chi^2$ probability $= 0.52$. Thus, we added the remaining 167 B14 galaxies and seven NED galaxies to our sample.

Our final spectroscopic catalogue includes 278 galaxies. The field of A1703 is covered by the SDSS. Its galaxy catalogue also provides us complete photometric information for all the galaxies of the spectroscopic sample in the magnitude bands *g*, *r*, and *i*.

Table 1 lists the velocity catalogue (see also Fig. 2): identification number of each galaxy, ID (Col. 1); redshift source (Col. 2; T:TNG, L:NED, B:B14); right ascension and declination, $\alpha$ and $\delta$ (J2000, Col. 3); (dereddened) SDSS *r* magnitude (Col. 4); heliocentric radial velocities, $V = cz_{\odot}$ (Col. 5) with errors, $\Delta V$ (Col. 6).

### 2.1 Notable galaxies

A1703 is dominated by the galaxy ID 141 (the BCG). It is by far the brightest cluster member, being the magnitude difference with the second brightest member galaxy ∼1.3. Its colours ($g - r = 1.58$ and $r - i = 0.59$) well match the red sequences of cluster early-type galaxies (see our analysis of Section 5.2.1) and, consistently, its optical spectrum is that of an elliptical galaxy free of emission lines.

The field of A1703 is populated by several point-like radio sources. Rizza et al. (2003; see their table 3) report six sources from high spatial resolution (∼1.5 arcsec) VLA images at 20 cm. The counterparts of five of them are the member galaxies IDs. 113, 151, 163, 200, and 202 (see Fig. 1). The sixth one (n. 5 in table 3 of Rizza et al. 2003), at ∼5.7 arcsec SW of the BCG, is not listed in our spectroscopic catalogue. Since its photometric redshift is $0.24 \pm 0.04$ (from the SDSS), it is unclear whether it is a cluster member or a foreground object. Finally, at ∼5 arcmin NNW of the BCG there is another strong radio source whose possible optical

**Table 1.** Velocity catalogue of 278 spectroscopically measured galaxies in the field of A1703. IDs in italics refer to non-member galaxies. Galaxy ID 141 (in boldface) is the BCG.

| ID | Source | $\alpha, \delta$ (J2000) | $r$ | $V$ (km s$^{-1}$) | $\Delta V$ |
|---|---|---|---|---|---|
| *001* | B | 13 13 13.66, + 51 48 48.1 | 21.09 | 142 509 | 69 |
| *002* | B | 13 13 16.19, + 52 03 34.4 | 21.46 | 166 775 | 96 |
| *003* | B | 13 13 16.50, + 51 41 17.8 | 20.03 | 116 430 | 27 |
| *004* | B | 13 13 21.13, + 51 57 26.5 | 20.64 | 126 545 | 36 |
| *005* | B | 13 13 21.59, + 51 46 30.6 | 18.98 | 70 250 | 30 |
| *006* | B | 13 13 22.20, + 51 55 51.6 | 20.70 | 90 154 | 54 |
| *007* | B | 13 13 22.63, + 51 52 35.9 | 20.70 | 107 578 | 75 |
| *008* | B | 13 13 25.19, + 51 49 53.9 | 18.84 | 115 294 | 18 |
| *009* | B | 13 13 25.56, + 51 44 31.7 | 20.73 | 114 710 | 39 |
| *010* | B | 13 13 27.59, + 51 49 33.9 | 20.61 | 115 480 | 111 |
| *011* | B | 13 13 31.36, + 51 47 39.4 | 20.99 | 86 817 | 66 |
| *012* | B | 13 13 32.20, + 52 03 01.7 | 20.67 | 147 285 | 39 |
| *013* | B | 13 13 34.59, + 51 40 21.1 | 21.18 | 155 562 | 54 |
| *014* | B | 13 13 35.50, + 51 53 48.3 | 21.72 | 116 685 | 33 |
| *015* | B | 13 13 37.34, + 51 47 28.3 | 21.10 | 189 304 | 57 |
| *016* | B | 13 13 43.03, + 51 46 48.6 | 20.64 | 124 402 | 54 |
| *017* | B | 13 13 45.96, + 51 51 02.8 | 20.27 | 114 620 | 63 |
| 018 | B | 13 13 46.21, + 51 42 28.5 | 19.13 | 83 693 | 33 |
| *019* | B | 13 13 46.53, + 51 43 39.1 | 20.76 | 125 199 | 33 |
| *020* | B | 13 13 46.65, + 51 51 46.1 | 19.90 | 154 438 | 27 |
| *021* | B | 13 13 47.76, + 51 56 13.8 | 20.12 | 101 459 | 51 |
| *022* | B | 13 13 48.24, + 51 57 09.2 | 20.97 | 116 841 | 84 |
| *023* | B | 13 13 51.79, + 51 59 46.9 | 19.49 | 102 676 | 33 |
| 024 | B | 13 13 52.32, + 51 39 31.1 | 19.85 | 83 369 | 39 |
| *025* | B | 13 13 54.87, + 51 38 42.0 | 20.46 | 87 818 | 45 |
| 026 | B | 13 13 58.50, + 51 46 30.0 | 19.59 | 82 845 | 30 |
| *027* | B | 13 14 01.35, + 51 57 06.0 | 23.47 | 88 999 | 84 |
| *028* | B | 13 14 03.13, + 51 45 47.5 | 20.70 | 143 175 | 69 |
| *029* | B | 13 14 04.11, + 51 58 47.1 | 17.61 | 17 850 | 150 |
| 030 | B | 13 14 07.66, + 51 55 57.6 | 20.65 | 82 893 | 60 |
| *031* | B | 13 14 08.32, + 51 38 55.1 | 20.28 | 143 490 | 42 |
| *032* | B | 13 14 09.91, + 51 54 27.6 | 17.03 | 17 982 | 150 |
| *033* | B | 13 14 10.21, + 51 59 34.0 | 15.34 | 9875 | 150 |
| 034 | B | 13 14 11.77, + 52 04 28.2 | 19.49 | 83 207 | 36 |
| 035 | B | 13 14 14.92, + 51 59 20.6 | 20.54 | 81 654 | 48 |
| 036 | B | 13 14 15.76, + 51 47 25.5 | 20.39 | 84 610 | 42 |
| *037* | B | 13 14 16.22, + 51 39 20.6 | 21.10 | 151 044 | 45 |
| *038* | B | 13 14 16.99, + 51 41 18.2 | 17.37 | 30 336 | 150 |
| 039 | B | 13 14 17.60, + 51 50 45.7 | 20.69 | 84 365 | 42 |
| *040* | B | 13 14 17.76, + 51 57 03.2 | 15.98 | 17 586 | 150 |
| *041* | B | 13 14 17.93, + 51 59 45.5 | 18.29 | 230 894 | 150 |
| *042* | B | 13 14 20.11, + 51 59 09.1 | 20.87 | 103 548 | 63 |
| 043 | B | 13 14 21.80, + 51 54 28.3 | 19.60 | 82 689 | 27 |
| 044 | B | 13 14 22.78, + 51 48 55.1 | 20.03 | 83 906 | 42 |
| *045* | B | 13 14 23.69, + 51 41 55.0 | 17.35 | 30183 | 150 |
| 046 | B | 13 14 26.19, + 51 50 20.3 | 19.25 | 82 893 | 24 |
| *047* | B | 13 14 27.08, + 52 01 14.4 | 19.79 | 106 429 | 24 |
| *048* | B | 13 14 32.96, + 52 02 12.2 | 18.98 | 759 027 | 150 |
| 049 | B | 13 14 33.36, + 51 55 04.2 | 20.39 | 82 611 | 51 |
| 050 | B | 13 14 34.01, + 51 48 11.9 | 19.85 | 82 707 | 30 |
| *051* | B | 13 14 34.53, + 51 39 47.5 | 17.56 | 53 363 | 150 |
| *052* | B | 13 14 35.86, + 52 00 11.3 | 16.88 | 25 995 | 150 |
| 053 | B | 13 14 38.16, + 51 44 43.7 | 21.72 | 84 428 | 69 |
| 054 | B | 13 14 38.65, + 51 56 10.3 | 20.17 | 82 281 | 54 |
| *055* | B | 13 14 38.71, + 51 44 07.6 | 19.56 | 92 369 | 27 |
| *056* | L | 13 14 41.80, + 51 48 57.5 | 17.12 | 56 244 | 10 |
| 057 | B | 13 14 42.01, + 51 58 42.5 | 21.28 | 83 045 | 72 |
| *058* | L | 13 14 42.92, + 51 48 16.3 | 19.95 | 143 644 | 34 |
| 059 | B | 13 14 44.28, + 51 51 03.7 | 20.34 | 84 679 | 48 |
| *060* | B | 13 14 45.30, + 51 55 15.2 | 19.64 | 80 920 | 30 |
| *061* | B | 13 14 45.60, + 51 38 52.8 | 21.01 | 102 172 | 108 |

**Table 1** – *continued*

| ID | Source | $\alpha, \delta$ (J2000) | $r$ | $V$ (km s$^{-1}$) | $\Delta V$ |
|---|---|---|---|---|---|
| 062 | T | 13 14 45.78, + 51 51 05.3 | 19.96 | 85 369 | 130 |
| 063 | B | 13 14 46.37, + 51 47 52.0 | 20.15 | 84 134 | 39 |
| *064* | B | 13 14 47.76, + 51 43 43.1 | 21.59 | 143 346 | 54 |
| 065 | B | 13 14 48.48, + 51 52 46.5 | 20.90 | 82 956 | 69 |
| *066* | B | 13 14 48.94, + 52 03 24.4 | 17.77 | 90 741 | 150 |
| *067* | B | 13 14 49.29, + 51 40 48.0 | 17.63 | 29 904 | 150 |
| *068* | B | 13 14 49.50, + 52 02 23.0 | 16.78 | 52 874 | 150 |
| 069 | B | 13 14 50.39, + 51 58 46.2 | 20.58 | 82 485 | 42 |
| 070 | B | 13 14 50.66, + 52 00 58.7 | 21.08 | 82 488 | 72 |
| 071 | T | 13 14 51.28, + 51 50 07.2 | 20.29 | 83 357 | 77 |
| *072* | L | 13 14 51.28, + 51 50 11.3 | 20.41 | 168 269 | 38 |
| 073 | T | 13 14 51.41, + 51 49 41.3 | 19.28 | 81 636 | 50 |
| 074 | B | 13 14 52.38, + 51 48 14.6 | 20.60 | 85 846 | 66 |
| *075* | B | 13 14 52.39, + 52 02 20.8 | 19.17 | 102 700 | 18 |
| 076 | B | 13 14 52.73, + 51 40 31.2 | 18.23 | 85 060 | 21 |
| 077 | B | 13 14 52.84, + 51 52 41.4 | 20.34 | 83 657 | 51 |
| *078* | T | 13 14 53.56, + 51 52 19.4 | 19.79 | 52 842 | 62 |
| *079* | T | 13 14 54.53, + 51 52 21.5 | 20.72 | 17 931 | 145 |
| 080 | T | 13 14 54.68, + 51 50 55.8 | 19.58 | 81 561 | 58 |
| *081* | L | 13 14 54.73, + 51 53 16.9 | 16.85 | 53 548 | 10 |
| 082 | T | 13 14 55.33, + 51 47 53.0 | 18.79 | 84 662 | 75 |
| *083* | L | 13 14 55.38, + 51 51 46.9 | 21.25 | 184 791 | 104 |
| *084* | B | 13 14 55.51, + 51 41 03.0 | 19.65 | 576 687 | 150 |
| *085* | B | 13 14 55.52, + 52 03 45.2 | 20.44 | 90 810 | 51 |
| 086 | B | 13 14 55.69, + 51 47 19.0 | 19.91 | 81 514 | 30 |
| *087* | T | 13 14 55.79, + 51 53 02.6 | 20.32 | 53 080 | 100 |
| *088* | B | 13 14 55.85, + 51 54 28.4 | 20.72 | 80 851 | 66 |
| *089* | T | 13 14 56.12, + 51 52 57.2 | 19.38 | 53 618 | 90 |
| 090 | B | 13 14 56.25, + 51 53 09.9 | 20.99 | 81 151 | 60 |
| 091 | T | 13 14 56.40, + 51 50 52.4 | 20.87 | 80 925 | 122 |
| *092* | L | 13 14 56.83, + 51 48 53.0 | 20.79 | 733 766 | 263 |
| 093 | T | 13 14 56.90, + 51 51 00.5 | 19.84 | 82 293 | 77 |
| 094 | T | 13 14 57.88, + 51 51 41.8 | 20.46 | 81 642 | 115 |
| 095 | B | 13 14 58.09, + 51 49 16.2 | 21.19 | 86 520 | 180 |
| *096* | T | 13 14 58.76, + 51 52 14.0 | 19.39 | 53 872 | 41 |
| 097 | B | 13 14 58.77, + 51 44 22.6 | 20.42 | 83 594 | 33 |
| 098 | T | 13 14 58.77, + 51 49 50.9 | 19.30 | 84 116 | 70 |
| *099* | T | 13 14 59.06, + 51 53 13.5 | 18.20 | 52 547 | 39 |
| 100 | T | 13 14 59.15, + 51 51 38.4 | 20.15 | 81 889 | 72 |
| 101 | T | 13 14 59.32, + 51 49 46.6 | 20.01 | 80 833 | 115 |
| 102 | T | 13 14 59.54, + 51 49 57.8 | 21.11 | 83 505 | 137 |
| 103 | B | 13 14 59.56, + 51 47 52.3 | 21.06 | 82 725 | 63 |
| *104* | B | 13 14 59.56, + 52 02 44.4 | 19.70 | 102 763 | 27 |
| 105 | T | 13 14 59.91, + 51 50 10.7 | 20.59 | 85 323 | 125 |
| 106 | T | 13 15 00.12, + 51 49 05.7 | 20.00 | 83 368 | 90 |
| 107 | T | 13 15 00.12, + 51 50 30.5 | 19.89 | 81 193 | 97 |
| 108 | T | 13 15 00.56, + 51 50 03.0 | 20.84 | 86 270 | 190 |
| 109 | T | 13 15 02.01, + 51 51 06.5 | 19.72 | 81 248 | 53 |
| 110 | T | 13 15 02.02, + 51 47 47.7 | 20.40 | 84 399 | 102 |
| *111* | B | 13 15 02.22, + 51 42 37.4 | 19.99 | 90 645 | 45 |
| 112 | B | 13 15 02.25, + 51 49 51.3 | 21.27 | 81 154 | 180 |
| 113 | T | 13 15 02.41, + 51 50 19.3 | 19.09 | 81 157 | 65 |
| 114 | T | 13 15 02.51, + 51 52 19.6 | 21.10 | 84 816 | 135 |
| 115 | T | 13 15 02.87, + 51 51 48.3 | 20.50 | 81 548 | 145 |
| 116 | T | 13 15 02.89, + 51 49 43.8 | 20.41 | 84 247 | 105 |
| 117 | T | 13 15 03.02, + 51 47 02.8 | 20.07 | 84 860 | 100e |
| 118 | T | 13 15 03.03, + 51 48 50.5 | 20.76 | 86 609 | 117 |
| 119 | T | 13 15 03.14, + 51 46 31.5 | 19.55 | 84 175 | 55 |
| 120 | T | 13 15 03.19, + 51 49 56.7 | 18.76 | 81 117 | 67 |
| 121 | T | 13 15 03.32, + 51 50 22.2 | 21.26 | 82 004 | 117 |
| 122 | T | 13 15 03.33, + 51 50 29.7 | 20.58 | 81 617 | 56 |
| 123 | T | 13 15 03.39, + 51 51 33.6 | 20.20 | 80 986 | 97 |
| 124 | T | 13 15 03.57, + 51 52 38.1 | 18.07 | 82 492 | 36 |

**Table 1** – *continued*

| ID | Source | $\alpha, \delta$ (J2000) | $r$ | $V$ (km s$^{-1}$) | $\Delta V$ |
|---|---|---|---|---|---|
| 125 | T | 13 15 03.90, + 51 49 26.8 | 19.61 | 84 224 | 57 |
| 126 | T | 13 15 03.92, + 51 49 09.9 | 20.51 | 80 792 | 120 |
| 127 | T | 13 15 03.92, + 51 50 44.8 | 19.92 | 81 334 | 82 |
| 128 | B | 13 15 04.05, + 51 39 51.0 | 20.35 | 84 110 | 48 |
| 129 | T | 13 15 04.20, + 51 50 04.4 | 20.26 | 80 779 | 100 |
| 130 | B | 13 15 04.26, + 51 47 50.8 | 23.42 | 83 942 | 300 |
| 131 | T | 13 15 04.31, + 51 47 22.6 | 20.55 | 83 922 | 63 |
| *132* | T | 13 15 04.33, + 51 51 33.7 | 18.48 | 53 157 | 75e |
| 133 | T | 13 15 04.35, + 51 51 47.1 | 20.66 | 82 945 | 92 |
| 134 | T | 13 15 04.50, + 51 49 11.1 | 21.57 | 84 697 | 145 |
| 135 | T | 13 15 04.84, + 51 49 32.0 | 18.74 | 81 410 | 65 |
| 136 | T | 13 15 05.00, + 51 50 02.7 | 19.33 | 83 533 | 72 |
| 137 | B | 13 15 05.04, + 51 46 06.3 | 22.58 | 87 210 | 150 |
| 138 | T | 13 15 05.04, + 51 52 08.2 | 20.27 | 81 517 | 105 |
| 139 | T | 13 15 05.10, + 51 49 54.0 | 20.50 | 81 889 | 102 |
| 140 | B | 13 15 05.18, + 52 03 06.9 | 20.05 | 81 331 | 30 |
| **141** | T | 13 15 05.24, + 51 49 02.6 | 16.76 | 84 697 | 75 |
| 142 | T | 13 15 05.28, + 51 48 35.3 | 20.92 | 83 155 | 80 |
| 143 | T | 13 15 05.29, + 51 47 53.1 | 18.37 | 79 194 | 32 |
| 144 | B | 13 15 05.32, + 51 45 36.5 | 22.04 | 82 923 | 150 |
| 145 | T | 13 15 05.50, + 51 50 01.7 | 20.46 | 81 449 | 72 |
| 146 | T | 13 15 05.75, + 51 52 31.7 | 19.15 | 83 298 | 54 |
| 147 | T | 13 15 05.92, + 51 48 45.1 | 19.16 | 82 249 | 65 |
| 148 | T | 13 15 06.02, + 51 49 01.4 | 21.22 | 79 868 | 97 |
| 149 | T | 13 15 06.17, + 51 49 43.0 | 20.60 | 83 816 | 75 |
| 150 | T | 13 15 06.24, + 51 48 34.9 | 18.34 | 82 684 | 117 |
| 151 | L | 13 15 06.36, + 51 54 27.9 | 18.13 | 82 178 | 12 |
| *152* | T | 13 15 06.52, + 51 51 00.5 | 19.72 | 26 235 | 100e |
| 153 | T | 13 15 06.68, + 51 48 00.3 | 20.08 | 85 795 | 75 |
| *154* | T | 13 15 06.69, + 51 47 16.3 | 19.69 | 116 336 | 288e |
| 155 | T | 13 15 06.96, + 51 49 25.8 | 19.69 | 85 901 | 72 |
| 156 | T | 13 15 07.05, + 51 50 49.9 | 20.46 | 83 602 | 100 |
| 157 | T | 13 15 07.27, + 51 51 20.6 | 20.07 | 84 067 | 80 |
| 158 | T | 13 15 07.41, + 51 48 22.6 | 19.05 | 85 381 | 37 |
| 159 | T | 13 15 07.43, + 51 48 37.9 | 21.34 | 83 013 | 102 |
| 160 | B | 13 15 07.45, + 51 39 35.6 | 20.00 | 84 730 | 51 |
| 161 | T | 13 15 07.47, + 51 47 36.2 | 20.81 | 83 184 | 105 |
| *162* | T | 13 15 07.71, + 51 51 03.4 | 17.80 | 25 921 | 100e |
| 163 | T | 13 15 07.83, + 51 48 58.0 | 18.55 | 84 172 | 62 |
| 164 | T | 13 15 08.08, + 51 48 48.6 | 19.19 | 84 643 | 82 |
| 165 | T | 13 15 08.08, + 51 53 08.0 | 18.93 | 85 814 | 49 |
| 166 | T | 13 15 08.11, + 51 52 17.0 | 20.64 | 81 998 | 97 |
| 167 | T | 13 15 08.19, + 51 51 53.9 | 18.88 | 82 376 | 42 |
| 168 | T | 13 15 08.21, + 51 48 28.9 | 20.78 | 87 478 | 106 |
| 169 | B | 13 15 08.83, + 51 45 45.5 | 23.01 | 83 372 | 150 |
| 170 | B | 13 15 08.91, + 51 46 22.4 | 22.31 | 81 094 | 150 |
| 171 | T | 13 15 08.91, + 51 49 06.7 | 20.99 | 82 229 | 180 |
| 172 | T | 13 15 09.01, + 51 49 55.8 | 20.43 | 87 915 | 112 |
| 173 | T | 13 15 09.40, + 51 47 21.7 | 19.78 | 84 361 | 55 |
| 174 | T | 13 15 09.76, + 51 48 21.5 | 20.74 | 81 446 | 107e |
| *175* | T | 13 15 09.97, + 51 53 31.5 | 21.04 | 184 767 | 60 |
| *176* | T | 13 15 10.01, + 51 52 43.6 | 20.31 | 124 393 | 165 |
| 177 | B | 13 15 10.05, + 51 43 13.3 | 20.20 | 83 252 | 45 |
| *178* | T | 13 15 10.11, + 51 52 23.2 | 19.87 | 93 275 | 107 |
| 179 | T | 13 15 10.15, + 51 50 03.2 | 19.31 | 82 684 | 117 |
| *180* | T | 13 15 10.18, + 51 53 20.0 | 19.93 | 52 960 | 100e |
| *181* | T | 13 15 11.06, + 51 49 03.2 | 17.82 | 52 937 | 62 |
| 182 | B | 13 15 11.06, + 51 46 53.8 | 21.97 | 80 644 | 180 |
| 183 | B | 13 15 11.07, + 51 45 57.7 | 21.36 | 82 923 | 150 |
| 184 | B | 13 15 11.19, + 51 48 23.3 | 20.73 | 85 069 | 63 |
| 185 | B | 13 15 11.20, + 51 44 18.2 | 20.53 | 84 958 | 69 |
| 186 | T | 13 15 11.50, + 51 46 41.5 | 19.77 | 80 732 | 54 |
| 187 | T | 13 15 11.59, + 51 49 20.4 | 19.04 | 80 514 | 55 |

**Table 1** – *continued*

| ID | Source | $\alpha, \delta$ (J2000) | $r$ | $V$ (km s$^{-1}$) | $\Delta V$ |
|---|---|---|---|---|---|
| 188 | B | 13 15 11.96, + 51 45 53.0 | 20.55 | 81 891 | 54 |
| 189 | T | 13 15 12.03, + 51 47 22.4 | 19.55 | 81 821 | 72 |
| 190 | T | 13 15 13.47, + 51 50 04.9 | 19.04 | 86 158 | 57 |
| 191 | T | 13 15 13.56, + 51 49 49.2 | 19.34 | 82 611 | 65 |
| 192 | T | 13 15 13.73, + 51 49 39.5 | 20.39 | 85 308 | 80 |
| 193 | T | 13 15 13.73, + 51 49 55.1 | 20.18 | 83 418 | 125 |
| *194* | T | 13 15 13.73, + 51 51 50.1 | 20.91 | 795 600 | 335e |
| 195 | T | 13 15 13.98, + 51 49 10.8 | 19.75 | 80 841 | 90 |
| 196 | T | 13 15 14.53, + 51 50 03.3 | 19.63 | 81 590 | 50 |
| 197 | T | 13 15 14.69, + 51 48 17.7 | 20.18 | 82 642 | 100 |
| 198 | T | 13 15 14.72, + 51 47 20.1 | 20.43 | 82 698 | 102 |
| 199 | T | 13 15 14.81, + 51 48 30.1 | 20.36 | 79 793 | 72 |
| 200 | T | 13 15 15.18, + 51 48 04.1 | 18.90 | 82 526 | 62 |
| 201 | T | 13 15 16.11, + 51 47 46.8 | 19.66 | 85 026 | 65 |
| 202 | T | 13 15 16.29, + 51 50 23.4 | 18.86 | 82 002 | 52 |
| 203 | B | 13 15 17.14, + 51 57 05.6 | 19.90 | 84 035 | 33 |
| *204* | B | 13 15 17.17, + 51 53 57.6 | 19.44 | 80 425 | 24 |
| *205* | B | 13 15 17.62, + 51 42 00.2 | 22.14 | 207 031 | 45 |
| *206* | T | 13 15 17.69, + 51 47 25.6 | 20.32 | 116 791 | 88 |
| 207 | B | 13 15 18.03, + 52 00 55.0 | 19.80 | 82 938 | 30 |
| *208* | B | 13 15 18.38, + 51 51 41.3 | 20.21 | 102 454 | 30 |
| 209 | T | 13 15 18.91, + 51 48 43.7 | 19.48 | 85 388 | 60 |
| 210 | T | 13 15 19.72, + 51 48 08.1 | 19.66 | 82 082 | 70 |
| *211* | B | 13 15 19.98, + 51 38 42.0 | 19.81 | 91 425 | 42 |
| 212 | B | 13 15 20.01, + 51 43 40.5 | 21.30 | 84 344 | 102 |
| 213 | B | 13 15 21.87, + 51 49 03.7 | 19.06 | 82 020 | 33 |
| *214* | B | 13 15 23.11, + 52 01 25.3 | 16.85 | 17 784 | 150 |
| *215* | B | 13 15 24.09, + 52 03 59.1 | 15.75 | 18 020 | 150 |
| 216 | T | 13 15 24.22, + 51 48 18.1 | 19.67 | 82 459 | 77 |
| *217* | B | 13 15 24.90, + 51 54 58.9 | 16.80 | 34 545 | 150 |
| 218 | B | 13 15 25.33, + 51 51 06.1 | 19.12 | 86 208 | 27 |
| 219 | T | 13 15 26.22, + 51 47 55.6 | 19.80 | 85 366 | 82 |
| *220* | B | 13 15 26.50, + 51 44 53.0 | 20.06 | 79 502 | 30 |
| 221 | B | 13 15 26.86, + 51 43 26.6 | 19.66 | 84155 | 30 |
| *222* | B | 13 15 28.43, + 51 37 52.7 | 21.40 | 137 335 | 111 |
| *223* | B | 13 15 29.91, + 51 52 57.7 | 21.08 | 135 929 | 48 |
| 224 | B | 13 15 29.93, + 51 55 44.0 | 19.58 | 84 053 | 30 |
| 225 | B | 13 15 31.56, + 51 45 34.0 | 21.26 | 82 521 | 54 |
| 226 | B | 13 15 33.48, + 51 51 16.1 | 21.35 | 84 607 | 63 |
| 227 | B | 13 15 33.75, + 51 58 54.8 | 20.39 | 81 948 | 39 |
| *228* | B | 13 15 43.19, + 51 49 50.2 | 20.19 | 116 071 | 54 |
| *229* | B | 13 15 44.27, + 51 43 33.4 | 19.18 | 86 715 | 30 |
| 230 | B | 13 15 45.61, + 51 52 01.9 | 19.19 | 82 593 | 27 |
| *231* | B | 13 15 45.69, + 52 00 28.3 | 22.39 | 304 781 | 93 |
| 232 | B | 13 15 46.20, + 51 48 23.5 | 19.14 | 84 032 | 24 |
| 233 | B | 13 15 46.60, + 51 51 25.2 | 19.36 | 82 686 | 24 |
| *234* | B | 13 15 50.10, + 51 39 16.0 | 20.85 | 129 262 | 57 |
| *235* | B | 13 15 51.52, + 51 48 47.4 | 19.80 | 78 333 | 33 |
| *236* | B | 13 15 52.41, + 51 44 41.9 | 21.29 | 159 684 | 45 |
| *237* | B | 13 15 52.41, + 51 46 41.6 | 20.63 | 102 907 | 51 |
| *238* | B | 13 15 53.47, + 51 56 58.1 | 20.38 | 132 484 | 18 |
| *239* | B | 13 15 55.87, + 51 53 13.3 | 20.10 | 56 832 | 36 |
| *240* | B | 13 15 59.50, + 52 04 14.3 | 20.44 | 95 229 | 45 |
| *241* | B | 13 16 00.79, + 51 51 07.8 | 17.12 | 56 613 | 150 |
| *242* | B | 13 16 01.28, + 51 57 00.4 | 20.38 | 132 517 | 45 |
| *243* | B | 13 16 04.09, + 51 43 47.0 | 21.54 | 117 054 | 63 |
| *244* | B | 13 16 08.41, + 51 40 25.6 | 20.93 | 89 371 | 75 |
| *245* | B | 13 16 13.15, + 52 03 27.8 | 19.93 | 116 766 | 30 |
| *246* | B | 13 16 13.47, + 52 04 54.6 | 20.95 | 100 044 | 63 |
| *247* | B | 13 16 13.62, + 51 45 08.0 | 21.08 | 102 475 | 57 |
| *248* | B | 13 16 13.79, + 51 40 25.9 | 20.12 | 89 287 | 48 |
| *249* | B | 13 16 15.13, + 51 38 48.8 | 17.37 | 7414 | 150 |
| *250* | B | 13 16 17.09, + 51 49 02.3 | 15.92 | 30 006 | 150 |

**Table 1** – *continued*

| ID | Source | $\alpha, \delta$ (J2000) | $r$ | $V$ (km s$^{-1}$) | $\Delta V$ |
|---|---|---|---|---|---|
| *251* | B | 13 16 17.12, + 51 40 34.4 | 18.07 | 89 866 | 150 |
| *252* | B | 13 16 17.61, + 51 40 32.8 | 21.62 | 89 671 | 48 |
| *253* | B | 13 16 19.78, + 51 37 59.5 | 19.42 | 96 146 | 30 |
| *254* | B | 13 16 21.77, + 51 56 56.8 | 20.48 | 97 516 | 54 |
| *255* | B | 13 16 22.55, + 52 01 04.1 | 19.61 | 109 346 | 30 |
| *256* | B | 13 16 24.13, + 51 49 42.9 | 20.99 | 142 701 | 48 |
| *257* | B | 13 16 24.73, + 51 38 19.0 | 20.60 | 122 696 | 18 |
| *258* | B | 13 16 25.12, + 51 55 06.6 | 20.19 | 102 853 | 39 |
| *259* | B | 13 16 26.10, + 51 50 24.7 | 20.34 | 100 245 | 33 |
| *260* | B | 13 16 26.30, + 51 41 28.2 | 19.80 | 108 648 | 36 |
| *261* | B | 13 16 28.11, + 52 00 23.2 | 21.30 | 109 409 | 63 |
| *262* | B | 13 16 29.73, + 52 03 47.4 | 19.42 | 117 642 | 27 |
| *263* | B | 13 16 33.53, + 51 51 53.8 | 21.20 | 100 386 | 78 |
| *264* | B | 13 16 34.26, + 52 00 07.7 | 20.16 | 118 847 | 15 |
| *265* | B | 13 16 35.47, + 51 54 28.7 | 23.11 | 185 215 | 89 |
| *266* | B | 13 16 37.66, + 51 55 11.8 | 19.93 | 90 768 | 33 |
| 267 | B | 13 16 41.40, + 52 02 21.2 | 19.89 | 83 510 | 39 |
| *268* | B | 13 16 41.45, + 51 57 22.0 | 20.07 | 118 202 | 27 |
| *269* | B | 13 16 43.20, + 51 42 56.8 | 20.89 | 88 894 | 39 |
| *270* | B | 13 16 43.76, + 51 45 54.5 | 20.52 | 129 894 | 30 |
| *271* | B | 13 16 45.52, + 51 51 29.0 | 20.95 | 103 099 | 102 |
| *272* | B | 13 16 46.34, + 51 40 53.8 | 20.81 | 101 519 | 51 |
| *273* | B | 13 16 46.68, + 51 43 34.8 | 21.09 | 130 098 | 48 |
| *274* | B | 13 16 47.00, + 51 44 11.6 | 20.59 | 123 820 | 54 |
| *275* | B | 13 16 48.49, + 51 56 30.5 | 20.73 | 117 273 | 33 |
| *276* | B | 13 16 49.03, + 51 58 13.2 | 18.85 | 99 969 | 33 |
| *277* | B | 13 16 49.96, + 51 38 07.5 | 19.17 | 112 059 | 18 |
| 278 | B | 13 16 51.24, + 51 38 27.4 | 20.59 | 83 435 | 42 |

counterpart (highlighted by a black arrow on the top of Fig. 1) is also visible in the X-ray *Chandra* Image. Due to its faint magnitude ($r \sim$23 from CFHT/Megaprime archival data) we argue that this object is a background AGN.

## 3 REMOVAL OF NON-MEMBERS

The removal of non-member galaxies was performed by using the two-step method called 'P + G' (see e.g. Biviano et al. 2013), which combines the 1D adaptive-kernel method DEDICA (1D-DEDICA; Pisani 1993) and the 'shifting gapper' method (Fadda 1996). For the centre of A1703 we adopted the position of the BCG (RA = $13^{\rm h}15^{\rm m}05\overset{\rm s}{.}24$, Dec. = $+51^{\circ}49'02\overset{''}{.}6$, see Table 1). The 1D-DEDICA method detected A1703 as a peak in the velocity space populated by 170 galaxies (see Fig. 3). Then, we rejected 23 galaxies from this provisional list of cluster members by using the 'shifting gapper', which combines the spatial and velocity information. The final sample contains 147 member galaxies (87 of which observed at the TNG), whose projected phase space is shown in Fig. 4.

## 4 GLOBAL PROPERTIES OF THE VELOCITY DISTRIBUTION

The biweight routines by Beers, Flynn & Gebhardt (1990) provide robust estimates of the first moments of the velocity distribution. Our measurement of the mean velocity is $\langle V \rangle = 83\,119 \pm 47$ km s$^{-1}$ (or $\langle z \rangle = 0.2773 \pm 0.0002$). The global line-of-sight (LOS) velocity dispersion is $\sigma_{\rm v} = 1324^{+88}_{-71}$ km s$^{-1}$. Based on the $\sigma_{\rm v}$–$M_{200}$ relation of Munari et al. (2013), inferred from $\Lambda$-cold dark matter cosmological $N$-body and hydrodynamical simulations, we estimate a

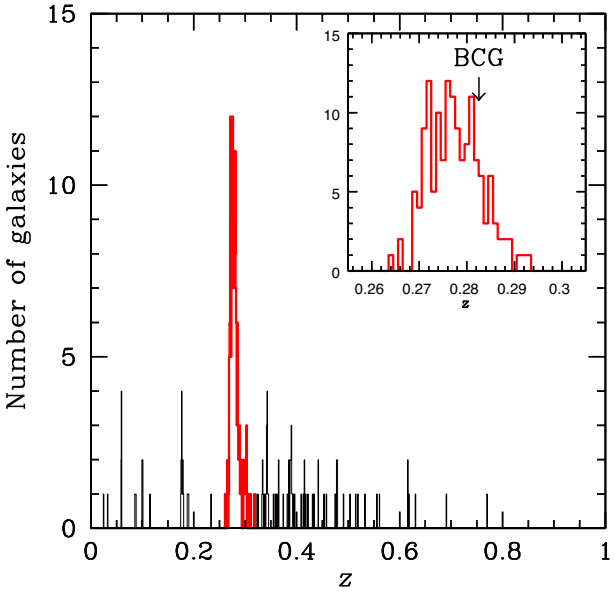


**Figure 3.** Redshift histogram of the galaxies of our spectroscopic sample. The solid red line histogram highlights the 170 galaxies assigned to A1703 by the 1D-DEDICA method. The distribution of the final 147 member galaxies with the indication of the BCG redshift is shown in the inset plot.

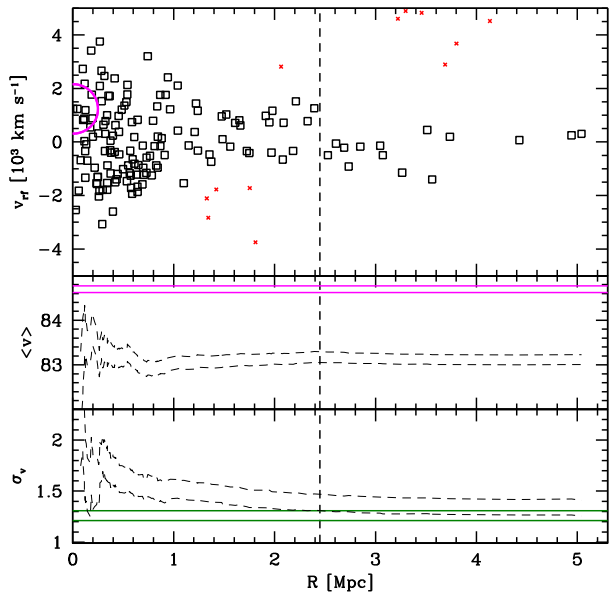


**Figure 4.** *Top panel*: Projected phase space diagram for the 147 member galaxies (squares) and non-members rejected with the shifting gapper procedure (small red crosses). Rest-frame LOS velocities are shown versus projected cluster-centric distance. The big magenta circle highlights the BCG. *Middle and Bottom panels*: Integral profiles of mean velocity and LOS velocity dispersion, respectively (only the one-$\sigma$ error bands are shown). The mean (and dispersion) at a given (projected) radius $R$ from the cluster-centre is estimated by considering all galaxies within that radius (the first value computed on the five galaxies closest to the centre). For all the panels, the vertical black dashed line indicates $R_{200}$. In the central panel, the horizontal magenta lines show the one-$\sigma$ error band of the BCG velocity. In the bottom panel, the horizontal green lines show the one-$\sigma$ error band of the *Chandra* X-ray temperature (from Ge et al. 2019, see Section 1) converted to $\sigma_{\rm v}$ (see Section 6 for details).

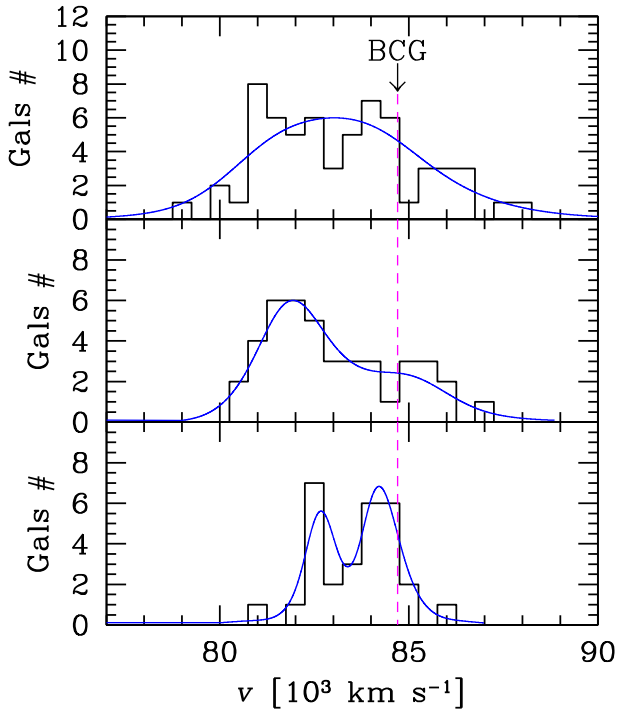


**Figure 5.** Velocity histogram of member galaxies in three projected cluster-centric distance intervals: 0–0.5 Mpc (*top panel*), 0.5–1 Mpc (*middle panel*), and 1–2.5 Mpc (*bottom panel*). For all panels, the blue curves show the number-galaxy density in the velocity space, as provided by the 1D-DEDICA method. The dashed magenta vertical line highlights the velocity of the BCG.

total cluster mass of $M_{200} = (2.2 \pm 0.6) \times 10^{15}\,M_{\odot}$ within $R_{200} = 2.45 \pm 0.15$ Mpc.

## 5 CLUSTER SUBSTRUCTURE

### 5.1 1D analysis of the velocity distribution

The 1D analysis refers to the study of the higher moments of the velocity distribution of member galaxies (Fig. 3). In particular, we find some evidence of deviation from Gaussianity according to the moments skewness and kurtosis (∼90–95 per cent and ∼90–99 per cent c.l., respectively). Moreover, there is also marginal evidence of asymmetry according to the asymmetry index (∼90–95 per cent c.l.; see Bird & Beers 1993 for details).

Very interestingly, the BCG has a significant (> 99 per cent c.l.) peculiar velocity $\Delta V_{\rm BCG}$ relative to the cluster mean velocity according to the Indicator test by Gebhardt & Beers (1991). In particular, the absolute $\sigma_{\rm v}$-normalized BCG peculiar velocity is $|\Delta V_{\rm BCG}|/\sigma_{\rm v} \sim 1.2$. This value puts the BCG of A1703 in the far tail of the $|\Delta V_{\rm BCG}|/\sigma_{\rm v}$ exponential distribution found by Lauer et al. (2014) studying a sample of 433 BCGs.

We then used the 1D-Kaye Mixture Model method (1D-KMM; Ashman, Bird & Zepf 1994). This test quantifies the statistical significance of bimodality (or more complex structure) in the velocity distribution with respect to a single Gaussian fit. The results are negative, i.e. there is no significant evidence of a two- or three-Gaussian partition. However, if we consider the velocity histograms obtained selecting member galaxies at different (projected) cluster-centric distances (see Fig. 5) we unveil a more complex reality. In fact, while in the centre of the cluster ($R \leq 0.5$ Mpc) the velocity distribution is fitted by 1D-DEDICA with a single peak curve, at larger cluster-centric distances signs of bimodality appear in the form of a fitted asymmetric curve. Then, for $R \gtrsim 1$ Mpc ($\sim 0.4\,R_{200}$), the velocity distribution is clearly described by a two-peak curve. The significance of the two peaks, at ∼82 700 and ∼84 200 km s$^{-1}$, is >99.4 per cent c.l. according to 1D-DEDICA.

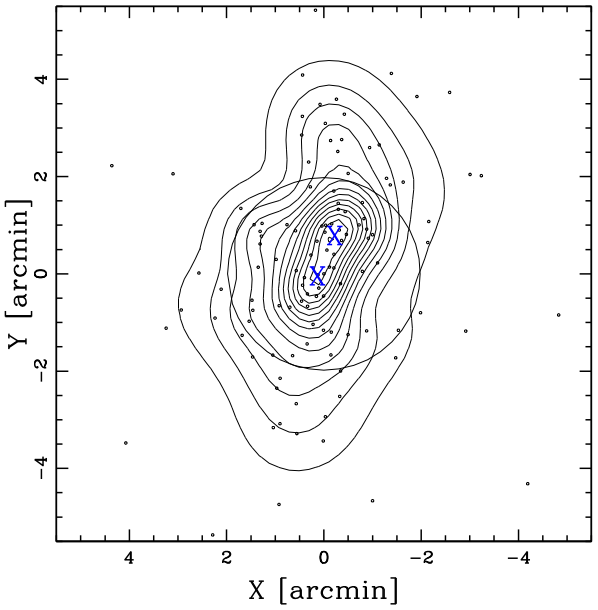


**Figure 6.** Spatial distribution of the spectroscopic cluster members in the central region of A1703 with, superimposed, the isodensity contour levels obtained with the 2D-DEDICA method. The blue crosses indicate the locations of the two galaxy peaks 'S' and 'N' (see also Table 2). The plot is centred on the cluster centre (the BCG) and circle contains the cluster within a radius equal to 0.5 Mpc.

**Table 2.** Substructures detected by the analysis of the 2D distribution of the spectroscopic members of A1703. For each subclump, the 2D-DEDICA method provides the number of assigned member galaxies $N_{\rm S}$, right ascension, and declination of the density peak, the relative density with respect to the densest subclump $\rho_{\rm S}$, and the $\chi^2$ value of the galaxy peak.

| Subclump | $N_{\rm S}$ | $\alpha$(J2000), $\delta$(J2000) h : m : s, ° : ′ :″ | $\rho_{\rm S}$ | $\chi^2_{\rm S}$ |
|---|---|---|---|---|
| N | 60 | 13 15 03.8, + 51 49 50 | 1.00 | 33.9 |
| S | 59 | 13 15 06.1, + 51 49 00 | 0.95 | 27.4 |

### 5.2 2D analysis of the galaxy distribution

About the analysis of the 2D spatial distribution of the spectroscopic member galaxies, we employed the 2D adaptive-kernel method of Pisani et al. (1996, hereafter 2D-DEDICA). The results are shown in Fig. 6. The cluster is elongated along the SSE-NNW direction, in a similar way to the X-ray isophotes (see Fig. 1). Moreover, this test detects two dense galaxy peaks separated by only $\lesssim$1 arcmin. The peak 'S' (see Table 2) is located close to the BCG (at ∼8 arcsec ESE), the peak 'N' is found at ∼9 arcsec SE of the galaxy ID 120. The eventual presence of luminosity segregation in a galaxy cluster can be a sign of disturbed dynamics (e.g. Maurogordato et al. 2011; see the discussion in Section 6). This motivates the exploration of the 2D galaxy distribution in different magnitude ranges. Very

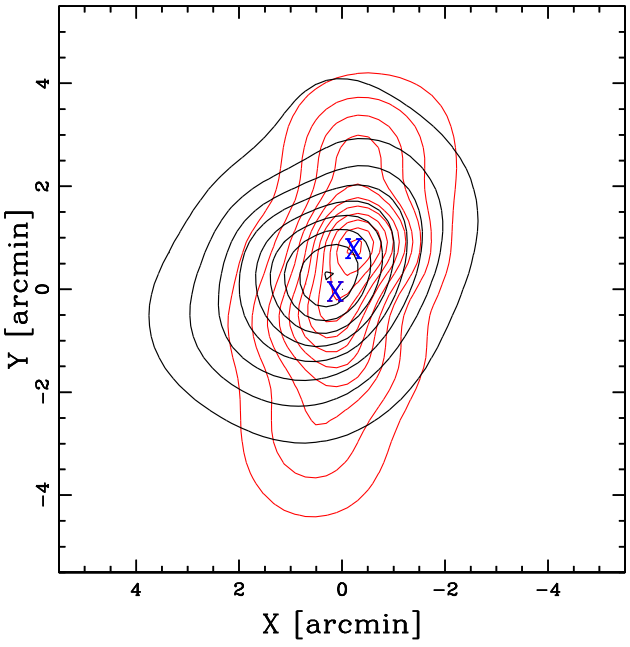


**Figure 7.** Isodensity contour map of the spectroscopic cluster members according to the 2D-DEDICA method. The black thick and red thin contours refer to bright ($r \leq 20$) and faint members, respectively (see the text). The blue crosses indicate the locations of the galaxy peaks 'S' and 'N' (see Table 2). The plot is centred on the cluster centre (the BCG).

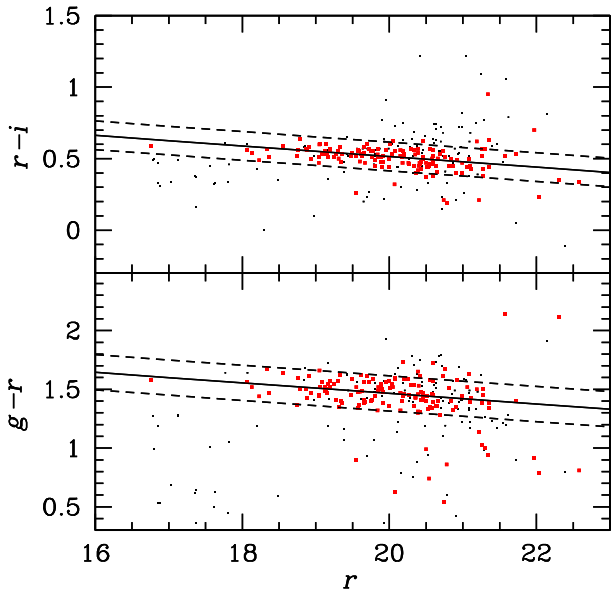


**Figure 8.** *Upper panel*: $r - i$ versus $r$ diagram for galaxies with available spectroscopic data. The red squares are cluster members, while black points represent field galaxies. The solid line shows the best-fitting CMR as computed from cluster members; the dashed lines are drawn at $r - i$ $\pm 0.1$ mag from the CMR (see the text). *Lower panel*: $g - r$ versus $r$ diagram for galaxies with available spectroscopic data. As above, the solid line shows the best-fitting CMR and the dashed lines are drawn at $g - r$ $\pm 0.15$ mag from the CMR.

interestingly, running 2D-DEDICA only on the bright spectroscopic members ($r \leq 20$) the result is completely different with respect to the analysis of the whole spectroscopic sample: the two peaks and the elongation disappear. The distribution of bright members is now much more circular (see Fig. 7) with a centre close to the BCG and to the peak 'S'. Moreover, the distribution of faint spectroscopic members shows a peak in correspondence of the peak 'N'.

### *5.2.1 Analysis of the photometric sample*

We are aware that the spectroscopic sample suffers from magnitude incompleteness. This is caused by constraints in the production process of the TNG MOS masks and the positioning of Hectospec fibres for the galaxies observed by B14.

The SDSS photometry of the cluster field is deep enough to help us alleviate our incompleteness problems. In particular, we select likely members on the basis of both ($r - i$ versus $r$) and ($g - r$ versus $r$) colour-magnitude relations (hereafter CMRs). The CMRs allow us to identify the cluster 'red' early-type galaxies (i.e. the dominant cluster population; Dressler 1980) and to reduce the contamination by non-member galaxies. We determine the CMRs by applying the $2\sigma$-clipping fitting procedure to the cluster members and obtain $r$–$i$ $= 1.255–0.037\times$ $r$ and $g$–$r$ $= 2.365–0.045\times$ $r$ (see Fig. 8). Then, within the photometric catalogue we consider as likely 'red' cluster members the galaxies with colour indexes $r$–$i$ and $g$–$r$ within 0.1 and 0.15 mag (i.e. the $1\sigma$-error associated to the fitted intercept) of the respective CMRs.

Fig. 9 shows the contour map of the likely cluster members according to 2D-DEDICA. Again, we find that the distribution of bright galaxies ($r \leq 20$) shows just one peak and is only mildly elongated. Only if we consider fainter members (galaxies with 20

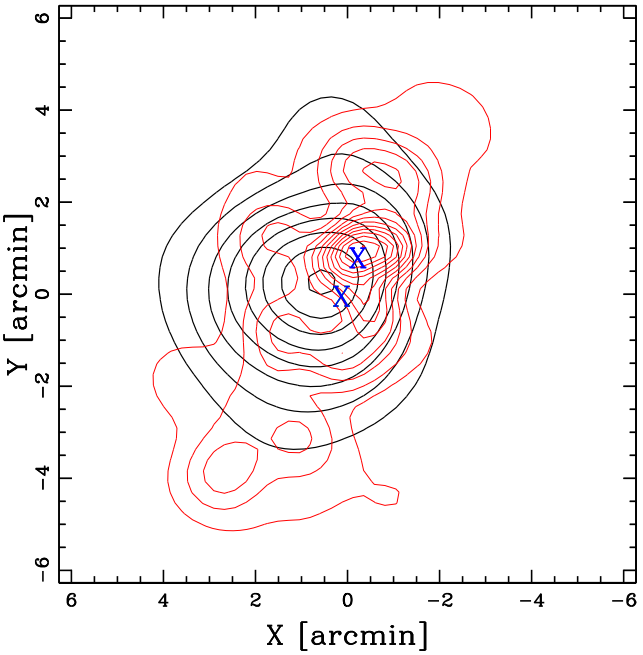


**Figure 9.** Isodensity contour map of the photometric likely cluster members according to the 2D-DEDICA method. The black thick and red thin contours refer to bright ($r \leq 20$) and faint members, respectively (see the text). The blue crosses indicate the locations of the galaxy peaks 'S' and 'N' (see Table 2). The plot is centred on the cluster centre (the BCG).

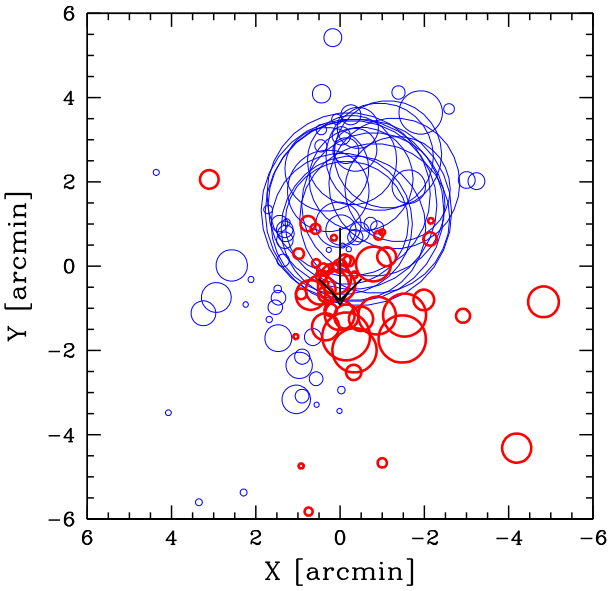


**Figure 10.** Spatial distribution of the cluster members in a 12 arcmin × 12 arcmin box, each marked by a circle: the larger the circle, the larger is the deviation of the local mean velocity from the global mean velocity. In particular, the thin/blue and thick/red circles show galaxies whose local value is smaller/larger than the global one according to the modified DS-test. The plot is centred on the cluster centre (the BCG). The black big arrow shows the direction of the velocity gradient (see the text).

$< r \leq 21.5$) we recover the SSE-NNW elongation with a maximum galaxy density close to the 'N' peak of Table 2.

This luminosity segregation is not a unique feature of A1703. In Section 6 we discuss this result in more detail.

### 5.3 3D analysis: combining velocity and position information

As for the 3D analysis, we employed different tools to search for a correlation between velocity and position information, which would be a clear sign of real substructures in the cluster.

First, we searched for an eventual velocity gradient by performing a multiple linear regression fit to the cluster velocity field (den Hartog & Katgert 1996). We find marginal evidence (at the ∼92 per cent c.l.) of a velocity gradient with PA $= 180 \pm 29$ degrees in the sample of the 147 spectroscopic cluster members. In particular, the southern region is populated by higher velocity galaxies.

Then, over the same sample we apply the classical Δ-test (Dressler & Schectman 1988, hereafter DS-test), which quantifies substructure searching for subsystems whose mean velocities and/or dispersions deviate from the global cluster values. Very significant substructure (at >99.9 per cent c.l., checked by running a Monte Carlo shuffling of the galaxy velocities; Dressler & Schectman 1988) is found in A1703 both with the 'canonical' DS-test and its modified version, which consider only the local mean velocity as kinematical indicator (see also e.g. Girardi, Boschin & Barrena 2010 for more details). Again, high velocity galaxies tend to populate the southern region of the cluster.

Later, we resorted to the 'hierarchical tree' (Htree) algorithm developed by Serna & Gerbal (1996; see also Adami et al. 2018 and Girardi et al. 2019 for recent applications). We apply it to the catalogue of 147 member galaxies. The method computes the relative binding energies of cluster galaxies and performs a hierarchical clustering analysis to detect galaxy subsystems.

The results of the Htree test are convincing: the cluster hosts two main substructures. In the centre of the dendrogram of Fig. 11 we find the group G2. It contains 35 galaxies and, in particular, the BCG. On the right the group G1 is the most prominent structure. It contains 47 galaxies and is itself substructured in two groups,

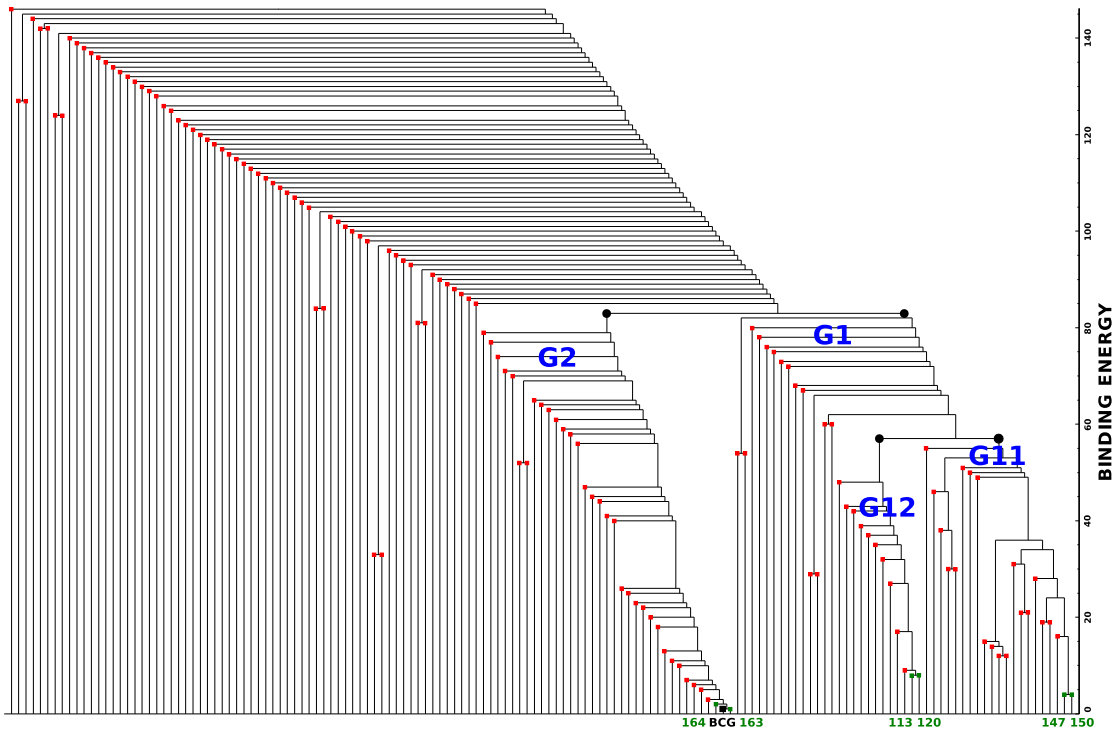


**Figure 11.** Dendrogram obtained through the Serna & Gerbal algorithm adopting $M/L_r = 150\,M_\odot/L_{r,\odot}$. The y-axis is the binding energy, here in arbitrary units with the lowest energy levels on the bottom. Labels indicate prominent galaxies and structures.

**Table 3.** Substructures detected by the 3D analysis of the spectroscopic members of A1703. For each subclump, the Htree method provides the number of assigned member galaxies $N_S$, the mean radial velocity with its error, and the radial velocity dispersion with its error.

| Subclump | $N_S$ | $\langle V \rangle$ km s$^{-1}$ | $\sigma_v$ km s$^{-1}$ |
|---|---|---|---|
| G1 | 47 | 82 022 ± 85 | 577 ± 48 |
| G2 | 35 | 84 681 ± 99 | 578 ± 75 |
| G11 | 21 | 82 466 ± 83 | 370 ± 69 |
| G12 | 12 | 81 242 ± 73 | 236 ± 72 |

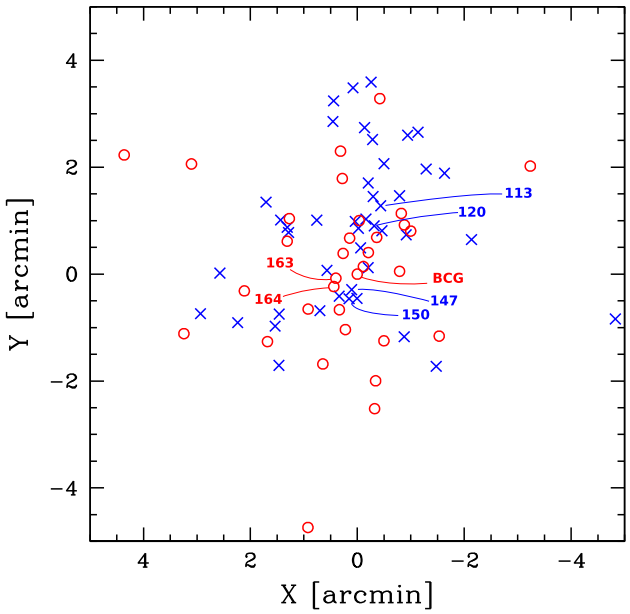


**Figure 12.** Member galaxies belonging to the groups G1 (blue crosses) and G2 (red circles) in a 10 arcmin × 10 arcmin box centred on the BCG. Labels highlight galaxies at the lowest binding energy levels of their respective groups (see Fig. 11).

G12 (12 galaxies) and G11 (21 galaxies). We run the Htree test by assuming a constant value of $M/L_r = 150\,M_\odot/L_{r,\odot}$ for the mass-to-light ratio of galaxies, but the results are quite robust against the adopted value of $M/L_r$.

In Table 3 we report the properties of the subclumps found with the Htree method.

In Fig. 12 we show the positions of the galaxies belonging to the groups G1 and G2. G1 galaxies have lower velocities and populate mainly the northern region of the cluster.

Note that the velocity dispersions of the groups of Table 3 are probably underestimated, since they do not include all the galaxies of the cluster and could just be the cores of more massive structures. To overcome this point we used the 3D version of the KMM test (3D-KMM). In particular, we used the galaxy assignments of the groups G1 and G2 as a first guess when fitting two groups. The algorithm fits a two groups partition at the 98.4 per cent c.l. The results for the two groups are reported in Table 4. Based on the estimates of the velocity dispersions of the two groups, we find from Munari et al. (2013): $R_{200} = 1.45 \pm 0.1$ Mpc and $M_{200} = (4.6 \pm 1.6) \times 10^{14}\,M_\odot$ for KMM3D1, $R_{200} = 1.6 \pm 0.2$ Mpc and $M_{200} = (5.8 \pm 2.6) \times 10^{14}\,M_\odot$ for KMM3D2. Therefore, the total mass would be $M_{200} = (10.4 \pm 3) \times 10^{14}\,M_\odot$.

**Table 4.** Substructures detected by the 3D analysis of the spectroscopic members of A1703. For each subclump, the 3D-KMM method provides the number of assigned member galaxies $N_S$, the mean radial velocity with its error, and the radial velocity dispersion with its error.

| Subclump | $N_S$ | $\langle V \rangle$ km s$^{-1}$ | $\sigma_v$ km s$^{-1}$ |
|---|---|---|---|
| KMM3D1 | 86 | 82119 ± 85 | 782 ± 66 |
| KMM3D2 | 61 | 84608 ± 109 | 845 ± 97 |

**Table 5.** Substructures detected by the 3D analysis of the spectroscopic members of A1703. For each subclump, the 3D-DEDICA method provides the number of assigned member galaxies $N_S$, the fitted radial velocity $V_{fit}$, right ascension, and declination of the density peak, the relative density with respect to the densest sub-clump $\rho_S$, and the $\chi^2$ value of the galaxy peak.

| Subclump | $N_S$ | $V_{fit}$ km s$^{-1}$ | $\alpha$(J2000), $\delta$(J2000) h : m : s, ° : ′ :″ | $\rho_S$ | $\chi^2_S$ |
|---|---|---|---|---|---|
| DED3D1 | 49 | 84 346 | 13 15 04.9, + 51 49 12 | 0.40 | 30 |
| DED3D2 | 43 | 81 242 | 13 15 02.8, + 51 50 16 | 1.00 | 44 |
| DED3D3 | 26 | 82 771 | 13 15 07.9, + 51 48 36 | 0.32 | 20 |

Finally, the substructure found by the Htree test is confirmed by the analysis performed with the 3D adaptive-kernel method of Pisani (1993, 1996; 3D-DEDICA). The results are reported in Table 5, where the three groups DED3D1, DED3D2, and DED3D3 correspond to the groups G2, G12, and G11 detected by the Htree method.

## 6 DISCUSSION AND CONCLUSIONS

The value of the global velocity dispersion $\sigma_v = 1324^{+88}_{-71}$ km s$^{-1}$ (in agreement with the estimate of B14) is typical of a massive cluster and is consistent with the X-ray temperature $kT_X = 9.63 \pm 0.75$ keV measured by Ge et al. (2019) under the assumption of energy density equipartition between galaxies and ICM. In fact, we find $\beta_{spec} = \sigma_v^2/(kT_X/\mu m_p) = 1.10^{+0.17}_{-0.15}$.

A value of $\beta_{spec} \sim 1$ is not anomalous for a dynamically relaxed cluster as A1703 was thought to be until very recently. However, we find convincing evidence that this cluster is experiencing a merger of two or more subclumps. The first hint of a disturbed dynamics comes from the 1D analysis of the galaxy velocity distribution. Even if its statistical moments suggest only marginal evidence of deviation from the Gaussianity, the velocity distributions of member galaxies at various cluster-centric distances (see Section 5.1 and Fig. 5) point out the possible existence of two galaxy populations with different mean velocities (separated by ∼2000 km s$^{-1}$) but well mixed in the central ($R \lesssim 1$ Mpc) region of the cluster. However, the most compelling argument in favour of an ongoing merger in A1703 comes from the very significant peculiar velocity of the BCG (e.g. Martel, Robichaud & Barai 2014). This is in sharp contrast with what is usually found in regular clusters, where the dominant galaxy is well placed at the peak of the global velocity distribution (as in the case e.g. of CL1821 + 643; Boschin et al. 2018).

About the 2D analysis of the galaxy distribution, the 2D-DEDICA method applied on the whole set of 147 member galaxies shows that the cluster is elongated in the SSE-NNW direction (Fig. 6) with two closely spaced peaks (see Table 2), another sign that at least two subclumps are in the process of merging. Indeed, if we consider

only bright members with $r \leq 20$, their spatial distribution is much more circular and exhibits only one peak close to the BCG and the peak 'S'. We remark that this luminosity segregation is confirmed also by the 2D analysis of the photometric members distribution, thus it does not seem an artefact of the incompleteness of the spectroscopic sample. Moreover, note that the peak 'N' and the density peak observed in the distribution of faint member galaxies (Figs 7 and 9) coincide with a secondary mass peak detected by Zitrin et al. (2010, see their fig. 7) from their lensing analysis. Such a spatial segregation between more and less luminous galaxies was found, for instance, in the Coma cluster (Biviano et al. 1996) and, in particular, in the merging cluster Abell 209 (Mercurio et al. 2003a), where bright photometric members are located around the dominant galaxy, while fainter galaxies seem to trace the whole cluster structure in agreement with the X-ray cluster morphology. As in the case of Abell 209 (see also Mercurio et al. 2003b), the segregation observed in A1703 could be interpreted as the result of a merging process caught after the core–core passage, where luminous galaxies trace the remnants of a pre-merging clump hosting the BCG.

Finally, the combined analysis of the velocity and spatial information provides the ultimate evidence of subclustering in A1703. In particular, the classical DS-test detects very significant substructure, with high velocity galaxies mostly located south of the BCG (Fig. 10). The Htree-test makes it possible to identify two main subclusters: G1 and G2 (Fig. 12 and Table 3). G2 hosts the BCG and is populated by high velocity galaxies. G1 exhibits a lower mean velocity and is itself substructured in two subgroups: G11 and G12. G12, in particular, hosts in the bottom of its potential well the galaxy ID 120, placed very close to the 'N' peak (Table 2). Comfortingly, the existence of G11, G12, and G2 is independently confirmed also by the 3D version of the adaptive kernel technique (see Table 5). The spatial distribution of G1 and G2 galaxies (see Fig. 12) explains the (marginal) evidence of a velocity gradient (Section 5.3) in the direction North–South and is in agreement with the results of the DS-test.

Using the galaxies assigned to G1 and G2 as a first guess when fitting a two groups partition, the 3D-KMM test divides the spectroscopic sample in two subclumps (Table 4). Based on their velocity dispersions we estimate a total mass $M_{200} \sim 1 \times 10^{15}\,M_{\odot}$ which should be interpreted as a lower limit for the mass of the cluster, being the upper limit $M_{200} \sim 2 \times 10^{15}\,M_{\odot}$ derived from the measurement of the global velocity dispersion (Section 4).

Now, we can adopt the above estimates for the mass of A1703 to study in more detail the merger of the two main subclusters G1 and G2. In particular, we use an analytical two-body model (see e.g. Lubin, Postman & Oke 1998 for the details of the method) which is based on the following parameters: $M_{\rm sys}$, the total mass of the system, $D$, the projected distance between G1 and G2, and $\Delta V_{\rm rf}$, the relative LOS velocity (in the rest frame). From the biweight estimate of the centres of G1 and G2 we assume $D = 0.46$ Mpc, while their relative velocity is $\Delta V_{\rm rf} \sim 2000\,{\rm km\,s^{-1}}$. If we also assume that we are seeing the two subclusters at $t = 0.3$ Gyr after the core crossing, which is a typical time suggested by the presence of the suspected radio halo in A1703 (e.g. Brunetti et al. 2009), we can plot a $M_{\rm sys}$ versus $\alpha$ (the projection angle between the plane of the sky and the vector defined by the centres of G1 and G2) graph for three types of solutions: Bound outgoing (expanding) solutions (BO), bound incoming (collapsing) solutions (BI), and unbound outgoing solutions (UO). The results are reported in Fig. 13. The only acceptable solutions in the estimated range of mass of A1703 are BO solutions with $\alpha \sim 65$–$70$ deg, i.e. we are seeing a merger quite close to the LOS. This is consistent with the hypothesis that the possible extended radio emission observed in the centre of the cluster is a radio halo. In fact, an eventual central radio relic produced by a shock wave propagating along the LOS is a rare event, being a relic preferentially observed in mergers occurring near the plane of the sky and in the outermost regions of a cluster (e.g. Vazza et al. 2012, Golovich et al. 2019).

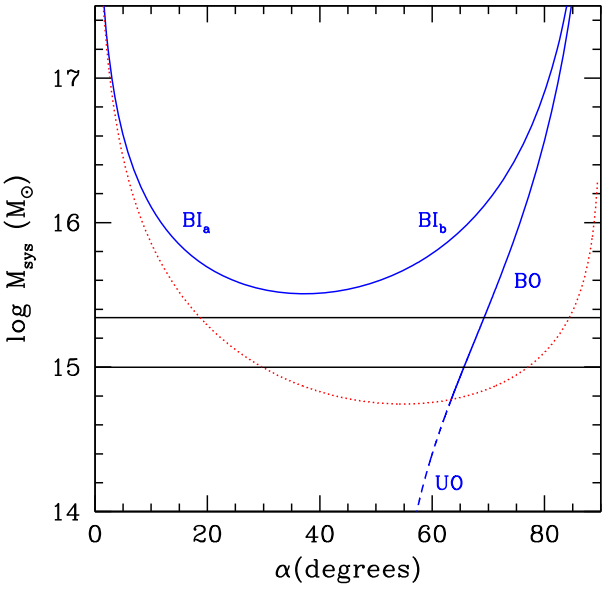


**Figure 13.** Bound and unbound solutions of the two-body model applied to the subclusters G1 and G2 (thick solid and dashed curves, respectively). The cluster mass is plotted versus the projection angle. Acceptable solutions are the curves intersecting the rectangle defined by the observational values of the cluster mass (bordered by the two horizontal lines). Regions above and below the thin dashed curve are the loci of bound and unbound solutions, respectively, according to the Newtonian criterion of gravitational binding (e.g. Beers, Geller & Huchra 1982).

In conclusion, the observational scenario suggests that A1703 is a massive cluster undergoing strong dynamical evolution, with two or three subclusters involved in a merging process. This evidence arises despite the cluster appears only slightly elongated in the X-rays, but this is not unusual. Indeed, a non-relaxed state is observed in ∼70 per cent of clusters at $z \sim 0.2$ even in the presence in some cases of a regular shape in the X-ray imaging data (Smith, Kneib & Smail 2005). Thus, our results are in agreement with the disturbed dynamics found by Ge et al. (2019) through the study of several X-ray morphological indicators.

In this merging context, the possible presence of a radio halo in the central regions of the cluster would not be surprising, thus we rule out the hypothesis that A1703 could constitute a new intriguing case of a rare relaxed cluster hosting diffuse radio emission.

Finally, our results are in marked contrast with respect to the picture of an unimodal, dynamically relaxed cluster painted by previous studies based on gravitational lensing (see Section 1). Since cluster mass profiles inferred from gravitational lensing suffer from complicated lens geometry (see Narayan & Bartelmann 1996 for a general review), if A1703 were a rare relaxed cluster at intermediate redshift it would be of great value to test structure formation in the ΛCDM paradigm through the study of its regular mass distribution. On the contrary, the subclustering we find in A1703 seems to rule out this possibility.

## ACKNOWLEDGEMENTS

We thank the anonymous referee for his/her stimulating comments and suggestions.

We are in debt with Federica Govoni for the VLA radio image she kindly provided us. We also thank Luigina Feretti for useful suggestions and discussions.

MG acknowledges financial support from the grant MIUR PRIN 2015 'Cosmology and Fundamental Physics: illuminating the Dark Universe with Euclid' and from the University of Trieste through the program 'Finanziamento di Ateneo per progetti di ricerca scientifica – FRA 2018'.

This publication is based on observations made on the island of La Palma with the Italian Telescopio Nazionale *Galileo*, which is operated by the Fundación Galileo Galilei-INAF (Istituto Nazionale di Astrofisica) and is located in the Spanish Observatorio of the Roque de Los Muchachos of the Instituto de Astrofísica de Canarias.

This research has also benefited from the galaxy catalogue of the Sloan Digital Sky Survey (SDSS). The SDSS web site is http://www.sdss.org/, where the list of the funding organizations and collaborating institutions can be found.

This research has made use of the NASA/IPAC Extragalactic Database (NED), which is operated by the Jet Propulsion Laboratory, California Institute of Technology, under contract with the National Aeronautics and Space Administration.

This research has also made use of IRAF. This package (ASCL code record 9911.002) is distributed by the National Optical Astronomy Observatory, which is operated by the Association of Universities for Research in Astronomy (AURA) under a cooperative agreement with the National Science Foundation.

## REFERENCES

Abell G. O., 1958, ApJS, 3, 211
Abell G. O., Corwin H. G. Jr., Olowin R. P., 1989, ApJS, 70, 1
Adami C. et al., 2018, A&A, 620, A5
Allen S. W., et al., 1992, MNRAS, 259, 67
Arnoud M., Pratt G. W., Piffaretti R., Böhringer H., Croston J. H., Pointecouteau E., 2010, A&A, 517, A92
Ashman K. M., Bird C. M., Zepf S. E., 1994, AJ, 108, 2348
Bayliss M. B., Johnson T., Gladders M. D., Sharon K., Oguri M., 2014, ApJ, 783, 41( B14)
Beers T. C., Geller M. J., Huchra J. P., 1982, ApJ, 257, 23
Beers T. C., Flynn K., Gebhardt K., 1990, AJ, 100, 32
Bird C. M., Beers T. C., 1993, AJ, 105, 1596
Biviano A., Durret F., Gerbal D., Le Fevre O., Lobo C., Mazure A., 1996, A&A, 311, 95
Biviano A. et al., 2013, A&A, 558, A1
Böhringer H., Chon G., Collins C. A., 2014, A&A, 570, A31
Bonafede A. et al., 2014, MNRAS, 444, L44
Boschin W., Girardi M., 2018, MNRAS, 480, 1187
Boschin W. et al., 2004, A&A, 416, 839
Boschin W., Girardi M., Barrena R., 2013, MNRAS, 434, 772
Brunetti G., Jones T. W., 2015, in Lazarian A., de Gouveia Dal Pino E. M., Melioli C., eds, Magnetic Fields in Diffuse Media, Astrophysics and Space Science Library, Vol. 407. Springer-Verlag, Berlin, Heidelberg, p. 557
Brunetti G., Cassano R., Dolag K., Setti G., 2009, A&A, 507, 661
Cassano R., Ettori S., Giacintucci S., Brunetti G., Markevitch M., Venturi T., Gitti M., 2010, ApJ, 721, L82
den Hartog R., Katgert P., 1996, MNRAS, 279, 349
Dressler A., 1980, ApJ, 236, 351
Dressler A., Shectman S. A., 1988, AJ, 95, 985
Fadda D., Girardi M., Giuricin G., Mardirossian F., Mezzetti M., 1996, ApJ, 473, 670
Feretti L., Giovannini G., Govoni F., Murgia M., 2012, A&ARv, 20, 54
Ge C. et al., 2019, MNRAS, 484, 1946
Gebhardt K., Beers T. C., 1991, ApJ, 383, 72
Girardi M., Boschin W., Barrena R., 2010, A&A, 517, A65
Girardi M., Bardelli S., Barrena R., Boschin W., Gastaldello F., Nonino M., 2011, A&A, 536, A89
Girardi M. et al., 2019, A&A, in press (eprint arXiv:1908.02277)
Gitti M., Brunetti G., Cassano R., Ettori S., 2018, A&A, 617, A11
Golovich N. et al., 2019, ApJ, 882, 69
Hennawi J. F. et al., 2008, AJ, 135, 664
Koester B. P. et al., 2007, ApJ, 660, 239
Lauer T. R., Postman M., Strauss M. A., Graves G. J., Chisari N. E., 2014, ApJ, 797, 82
Limousin M. et al., 2008, A&A, 489, 23
Lubin L. M., Postman M., Oke J. B., 1998, AJ, 116, 643
Mantz A. B., Allen S. W., Morris R. G., Schmidt R. W., von der Linden A., Urban O., 2015, MNRAS, 449, 199
Martel H., Robichaud F., Barai P., 2014, ApJ, 786, 79
Maurogordato S. et al., 2011, A&A, 525, A79
Mercurio A., Girardi M., Boschin W., Merluzzi P., Busarello G., 2003a, A&A, 397, 431
Mercurio A. et al., 2003b, A&A, 408, 57
Munari E., Biviano A., Borgani S., Murante G., Fabjan D., 2013, MNRAS, 430, 2638
Narayan R., Bartelmann M., 1996, lecture presented at the 13th Jerusalem Winter School in Theoretical Physics. Formation of Structure in the Universe, Jerusalem, Israel, 27 Dec 1995–5 Jan 1996
Navarro J. F., Frenk C. S., White S. D. M., 1997, ApJ, 490, 493
Oguri M. et al., 2009, ApJ, 699, 1038
Oguri M. et al., 2012, MNRAS, 420, 3213
Owen F., Morrison G., Voges W., 1999, Diffuse Thermal and Relativistic Plasma in Galaxy Clusters, MPE Report 271. p. 9
Piffaretti R. et al., 2011, A&A, 534, A109
Pisani A., 1993, MNRAS, 265, 706
Pisani A., 1996, MNRAS, 278, 697
Planck CollaborationXIII, 2016, A&A, 594, A27
Press W. H., Teukolsky S. A., Vetterling W. T., Flannery B. P., 2007, Numerical Recipes. The Art of Scientific Computing, 3rd edn. Cambridge University Press, Cambridge.
Richard J., Pei L., Limousin M., Jullo E., Kneib J.-P., 2009, A&A, 498, 37
Rizza E. et al., 2003, AJ, 126, 119
Sarazin C. L., 2002, in Feretti L., Gioia I. M., Giovannini G., eds, Merging Processes in Galaxy Clusters, Astrophysics and Space Science Library, Vol. 272. Springer, Berlin, p. 1
Savini F. et al., 2018a, MNRAS, 478, 2234
Savini F. et al., 2018b, MNRAS, 474, 5023
Serna A., Gerbal D., 1996, A&A, 309, 65
Smith G. P., Kneib J.-P., Smail I., 2005, MNRAS, 359, 417
Sommer M. W. et al., 2017, MNRAS, 466, 966
Tonry J., Davis M., 1979, ApJ, 84, 1511
van Haarlem M. P. et al., 2013, A&A, 556, A2
van Weeren R. J. et al., 2019, Space Sci. Rev., 215, 16
Vazza F. et al., 2012, MNRAS, 421, 1868
Venturi T. et al., 2017, A&A, 603, A125
Wilber A. G., 2018, PhD Thesis, University of Hamburg, Germany
Zitrin A. et al., 2010, MNRAS, 408, 1916

This paper has been typeset from a TEX/LATEX file prepared by the author.